Inventory, Distribution and Geometric Characteristics of Landslides in Dongchuan District, Yunnan Province, China

Shaochang Liu , Siyuan Ma , Xiaoli Chen *

Posted Date: 10 March 2026

doi: 10.20944/preprints202603.0694.v1

Keywords: landslide; distribution pattern; geometric characteristics

 doi:10.20944/preprints202603.0694.v1

Artilce

Inventory, Distribution and Geometric Characteristics of Landslides in Dongchuan District, Yunnan Province, China

Shaochang Liu [1,2], Siyuan Ma [3] and Xiaoli Chen [3,*]

1. Kunming Institute of Earthquake Forecast, China Earthquake Administration, Kunming 650224, China
2. Yunnan Earthquake Agency, Kunming, Yunnan 650224, China
3. Key Laboratory of Active Tectonics and Volcanic Hazards, Institute of Geology, China Earthquake Administration, Beijing, 100029, China

* Correspondence: chenxl@ies.ac.cn

Abstract

The Dongchuan District of Kunming City lies in the transition zone between the Yunnan-Guizhou Plateau and the Sichuan Basin, hosting numerous landslides that pose a serious threat to local lives and property. Therefore, compiling a comprehensive landslide inventory and analyzing the relationships between landslide spatial distribution and influencing factors are of significant importance for geological hazard prevention. This study focuses on the Dongchuan District. High-resolution remote sensing imagery was interpreted to establish a landslide inventory, and the spatial distribution and geometric characteristics of landslides were systematically analyzed. The results show that a total of 1,623 landslides were identified, covering an area of 10.36 km². Landslides predominantly occur at elevations of 1,000-2,000 m, on slopes of 20°-45°, with aspects of 255°-285°, relief between 150-400 m, annual rainfall below 825 mm, and within a distances of 1,000 m from rivers and 3,000 m from faults. Four landslide clusters were delineated along the Xiao River Fault, highlight the significant influence of the fault on the spatial distribution of landslides. Most landslides are longitudinal in planform, with travel distances (L) of 50-450 m and heights (H) from 25 to 350 m, exhibiting allometric relationships between these parameters and volume. The mean H/L ratio is 0.56 (corresponding to a mean reach angle of 29°), significantly higher than that observed in Baoshan City (mean reach angle of 21°). The results would be helpful for further understanding landslide initiation mechanisms and spatial distribution patterns on the northern margin of the Yunnan-Guizhou Plateau and providing valuable data support for subsequent landslide hazard risk assessment in this region.

Keywords: landslide; distribution pattern; geometric characteristics

1. Introduction

Landslides, resulting from the imbalance between crustal uplift and erosion in mountainous areas, significantly influence topographic development and landform evolution [1,2]. Existing studies demonstrate that topographic and geological factors critically govern slope stability, with landslide distribution patterns varying significantly across different terrain conditions, underscoring the complexity of landslide environments and their controlling factors [3–5].

A detailed and comprehensive landslide inventory serves as a crucial foundational dataset for analyzing landslide patterns and assessing hazard risk [6,7]. Yunnan is among the most landslide-prone provinces globally, where steep topography, neotectonic activity, seismicity, and intense precipitation create highly susceptible slope conditions [8]. In recent years, researchers have compiled extensive landslide inventories through visual interpretation of remote sensing images. For instance, Tian, et al. [9], He, et al. [10] , and Jin, et al. [11] developed coseismic landslide inventories for the Ludian *Ms* 6.5, Qiaojia *Ms* 5.1, and Yiliang *Ms* 5.6 earthquakes in northern Yunnan Province using

 doi:10.20944/preprints202603.0694.v1

high-resolution pre- and post-earthquake satellite imagery. Similarly, Shao, et al. [7] established a detailed landslide inventory for Baoshan City in western Yunnan by interpreting landslides from high-resolution Google Earth satellite images. However, the scarcity of regional landslide inventories has limited systematic comparative analyses of landslide spatial patterns and geometric characteristics across diverse geological settings.

The Dongchuan District of Kunming City is located in the transition zone between the Yunnan-Guizhou Plateau and the Sichuan Basin. Its distinctive terrain of high mountains and deep gorges, combined with intense tectonic activity and abundant rainfall, has created a fragile environment for slope rock and soil bodies, making it one of the areas that suffer from frequent and severe landslide hazards. For instance, in 2001, a landslide in Yingming township resulted in 14 fatalities, 22 injuries, and 7 missing (https://www.chinanews.com.cn/2001-07-10/26/103883.htm). Similarly, a landslide in the same township in 2014 caused 9 fatalities (https://inews.ifeng.com42363727/news.shtml). Despite these hazards, the region provides a natural laboratory for investigating the relationship between landslide spatial distribution and geomorphic setting.

While previous research has primarily focused on susceptibility and risk assessments of debris flows [12–16], as well as debris flow monitoring and kinematic characteristics [17–20]. Studies on the spatial distribution and geometric characteristics of landslides remain limited. To bridge this gap, this study establishes a detailed landslide inventory map and further analyzes the spatial distribution, geometric features, and influencing factors of these landslides. The results provide essential data support for assessing landslide hazard risk and understanding the impact of landslides on landform evolution.

2. Study Area

The Dongchuan District is situated in northeastern Yunnan Province, China, spanning longitudes from 102°47′ E to 103°18′ E and latitudes from 25°57′ N to 26°32′ N, covering a total area of 1,865.8 km². It borders Guizhou Province to the east, Huize County to the west, Luquan County and Xundian counties to the south, and Qiaojia County of Zhaotong City to the north (Figure 1). The Wumeng Mountains and Gongwang Mountains enclose the Xiao River, which flows through the entire territory from north to south, forming a distinctive alpine canyon landscape and contributing to high susceptibility to debris flows. This area is often referred to as the "World's Museum of Debris Flows". The topography of the study area is characterized by higher elevations in the northwest and lower elevations in the southeast; the altitude ranges from 695 m to 4,344 m, and it features a subtropical monsoon climate, with an average annual temperature of 14.9°C and an average annual precipitation of 1,000.5 mm, primarily concentrated from May to September (www.kmdc.gov.cn/c/2025-04-28/7002072.shtml).

 doi:10.20944/preprints202603.0694.v1

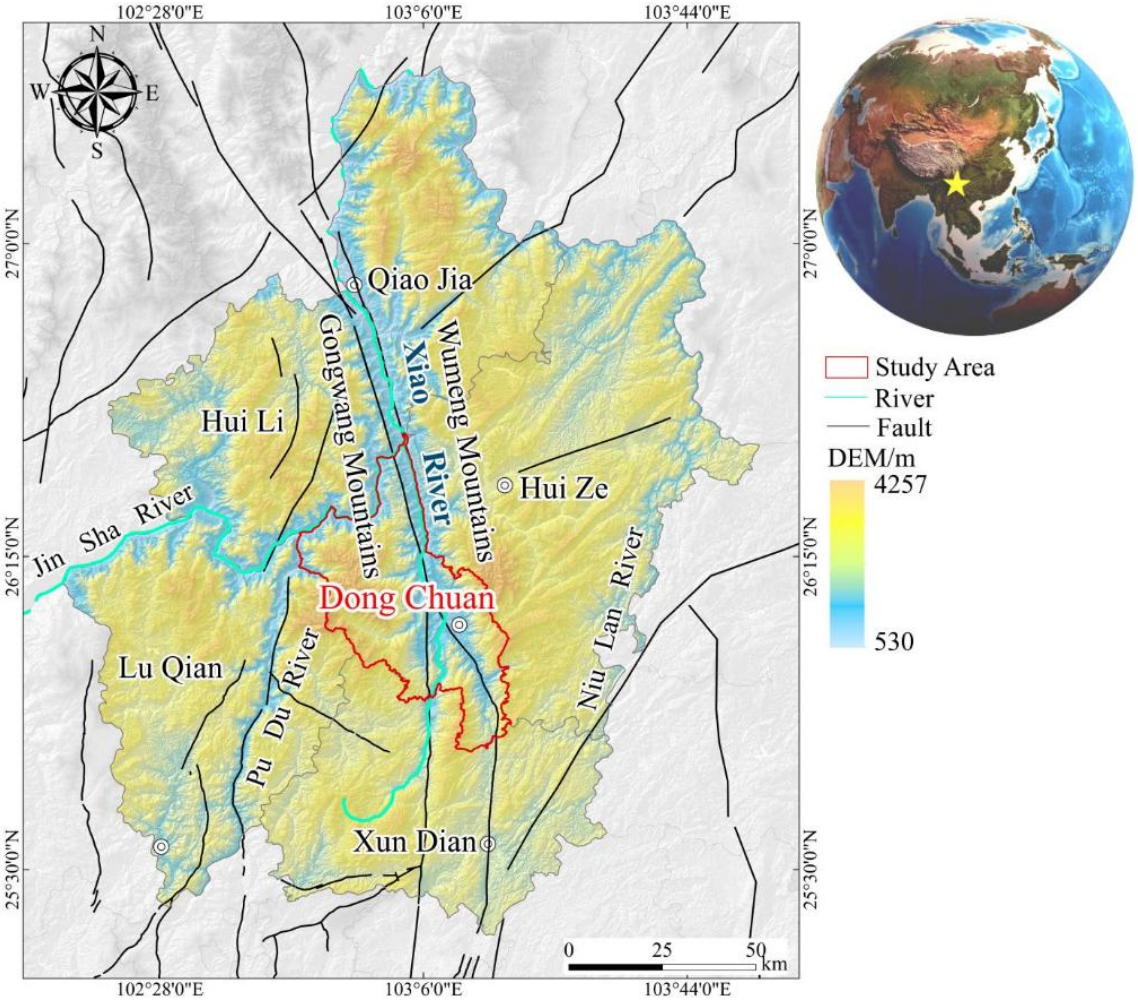

Figure 1. Map showing the location, topographic distribution, river system, and faults of the Dongchuan District and surrounding area. The red polygon denotes the study area; black lines denote faults; and green lines denote rivers.

Structurally, the region lies on the western margin of the Yangtze Block, where intense tectonic activity has led to the formation of numerous faults. Major faults include the Luoxue Fault (F1), Xindianfang Fault (F2), Xinlongcun Fault (F3), Western Branch of the Xiao River Fault (F4-1), Eastern Branch of the Xiao River Fault (F4-2), and the Yulu-Daibu Fault (F5) (Figure 2). These faults are primarily N-S to NNW striking, among them, the Xiao Rive Fault (F4-1 and F4-2) is the only active fault and is characterized by left-lateral strike-slip motion [21]. Since 1733, four earthquakes with *M*s > 5.0 have occurred in this region (Figure 2).

The stratigraphy of the study area is diverse, with exposed strata ranging from the Paleozoic Erathem to the Quaternary. To the west of the Western Branch of the Xiao River Fault (F4-1), the exposed strata primarily consist of Proterozoic (Pt), Cambrian (Є), Ordovician (O), Silurian (S), Permian (P), Triassic (T), Jurassic (J) and Quaternary (Q), while to the east, they are mainly composed of Paleozoic Erathem (Pz), Proterozoic (Pt), Devonian (D), Carboniferous (C), Permian (P), Jurassic (J), and Tertiary (N) and Quaternary(Q) (Figure 2).

 doi:10.20944/preprints202603.0694.v1

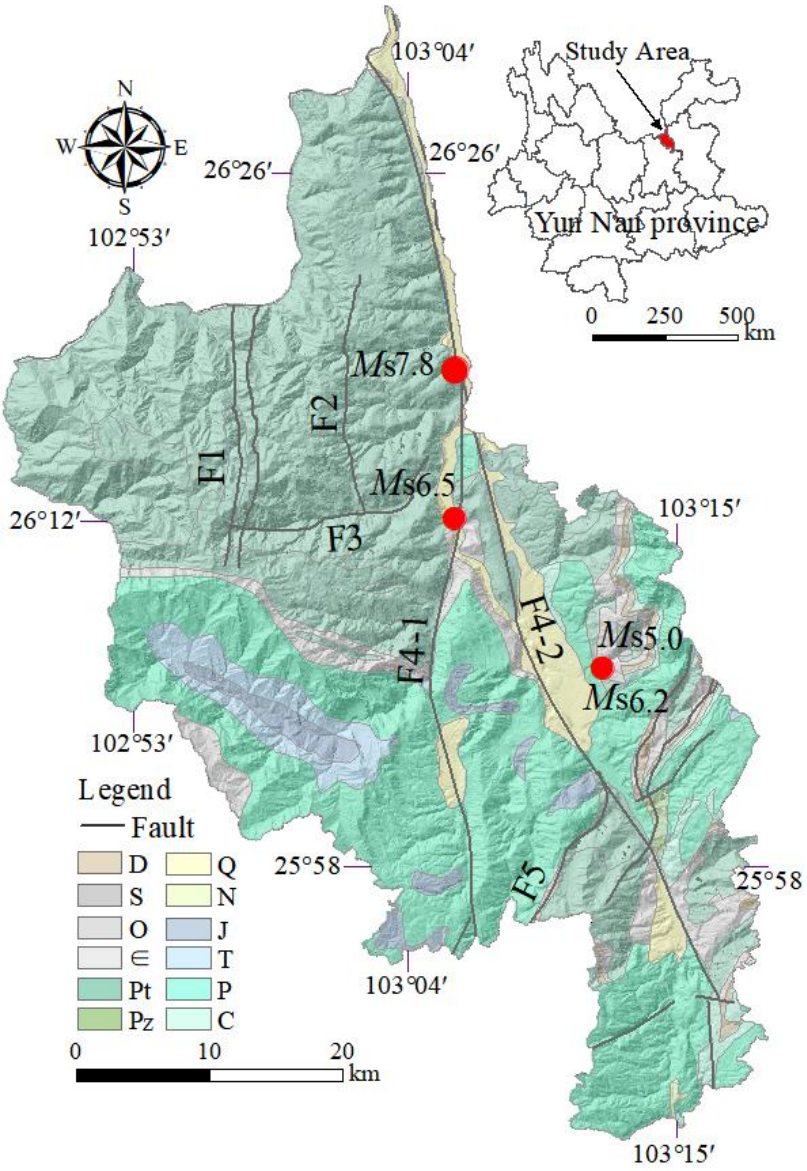

Figure 2. Map showing the stratigraphy, historical earthquakes, and faults of the Dongchuan District (F1: Luoxue Fault; F2: Xindianfang Fault; F3: Xinlongcun Fault; F4-1: Western Branch of the Xiao River Fault; F4-2: Eastern Branch of the Xiao River Fault; and F5: Yulu-Daibu Fault).

3. Methods and Data

3.1. Landslide Mapping

The Google Earth platform provides high-resolution satellite imagery and is widely used in landslide investigations [22–24]. In this study, landslides were identified and analyzed through visual interpretation of remote sensing imagery [25,26]. The high-resolution images were obtained from the Google Earth platform, spanning January 2020 to March 2025 with full spatial coverage (100%) of the study area. The interpretation focused on landslides within the Dongchuan District. By analyzing variations in color, texture, and topography, the boundaries and extents of the landslides were delineated using polygons. Each landslide was mapped through visual interpretation of multi-temporal images. In high-resolution imagery, most landslides appear as bright spots and preserve key geomorphic features such as landslide scarps, depressions, and accumulation bodies. These features exhibit distinct textures and spectral signatures that significantly differ from the surrounding environment (Figure 3).

 doi:10.20944/preprints202603.0694.v1

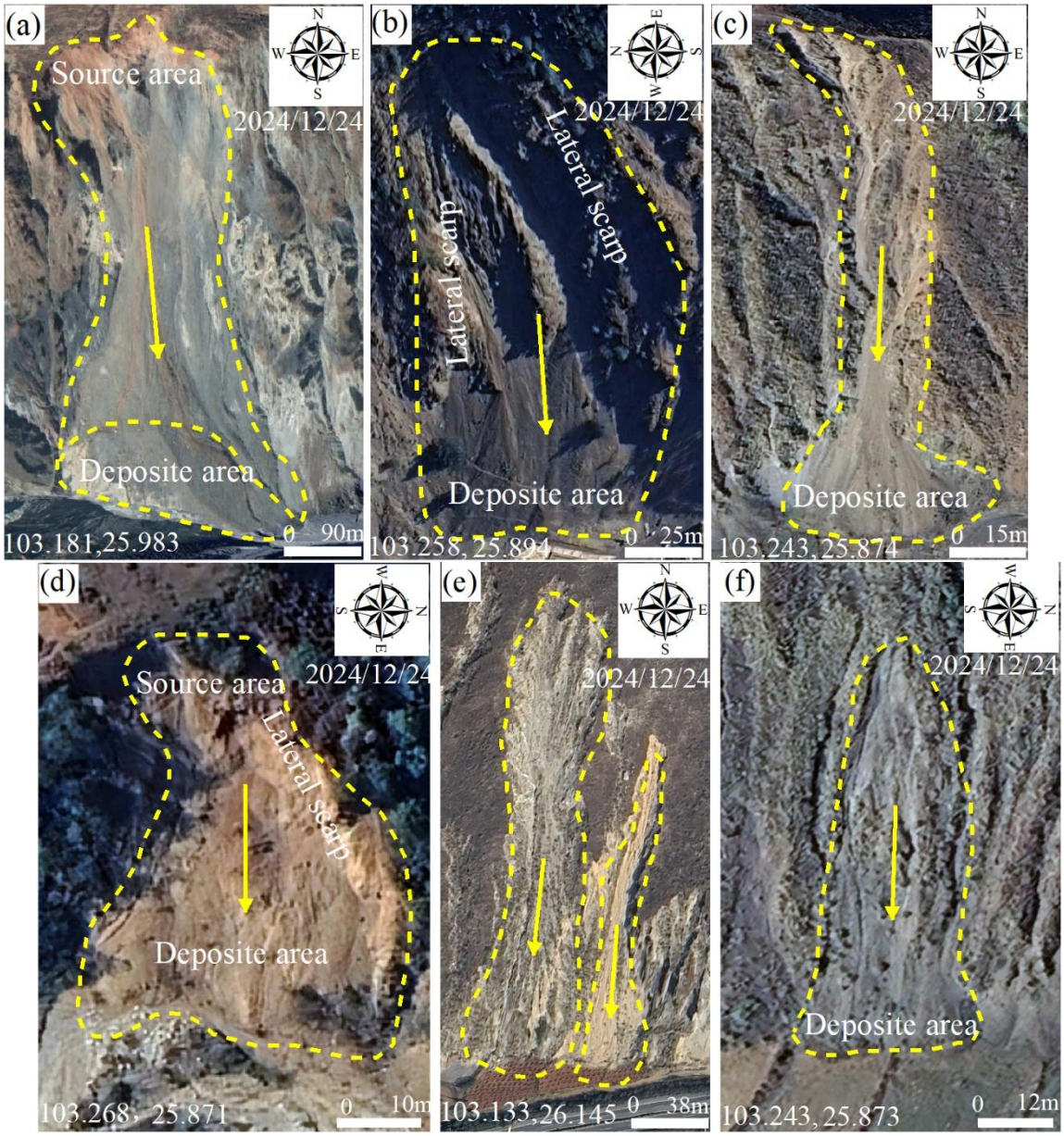

Figure 3. Typical landslides in the study area (satellite images from the Google Earth platform). The yellow polygons represent the interpreted landslide boundaries.

To ensure comprehensive and accurate landslide identification, a systematic interpretation was conducted across the entire study area. A grid-based approach was adopted using the latitude-longitude grid provided by Google Earth. During interpretation, a viewing altitude of approximately 1.5 km above ground level was maintained as the baseline. When landslide outlines were not clearly discernible at this scale, the view was magnified to delineate boundaries accurately. To ensure interpretation accuracy, the inventory was rigorously cross-checked to minimize omissions and commission errors.

3.2. Geometric Parameters of Landslides

Geometric parameters are fundamental for determining landslide types and understanding their kinematic characteristics [27,28]. Among these, the length-to-width ratio (L/W) reflects the geometrical shape of a landslide, while the height-to-length ratio (H/L) and the reach angle (arctan (H/L)) represent landslide mobility [28]. In this study, the height (H) is defined as the elevation difference between the landslide crown and toe along the direction of movement (Figure 4b,d). The

 doi:10.20944/preprints202603.0694.v1

length (L) refers to the minimum distance from the crown to the toe along the sliding direction, and the width (W) is the maximum breadth perpendicular to the length (L) (Figure 4b-d, 5) [29].

The volume of landslides is calculated using the following empirical formula [30], which was derived from a comprehensive global dataset comprising 4,231 landslide records. This formula has been validated across diverse physiographic settings and is widely adopted in the literature [31–34], demonstrating its applicability and suitability for our research needs. In this formula, V is the estimated landslide volume, and A is the landslide area.

$$V_L = \alpha A^{\beta} \quad (\alpha = 0.146,\ \beta = 1.332)$$

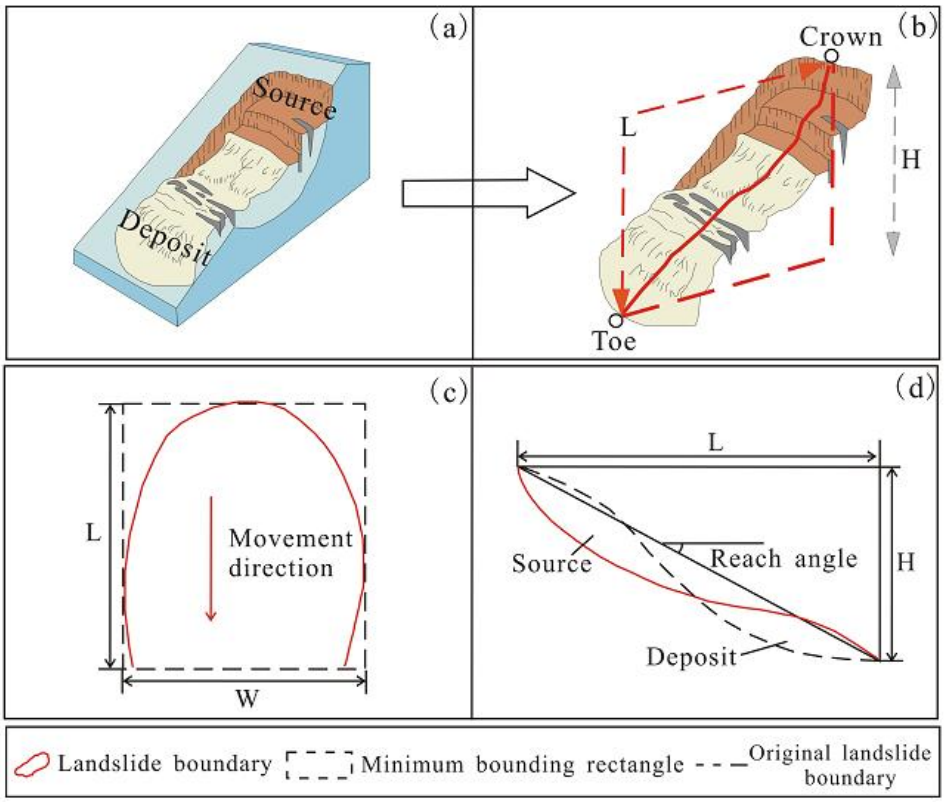

Figure 4. (a) Landslide slope position [35]; (b) Landslide length and height map [35]; (c) Landslide length and width [36]; (d) Landslide height and the reach angle [37].

 doi:10.20944/preprints202603.0694.v1

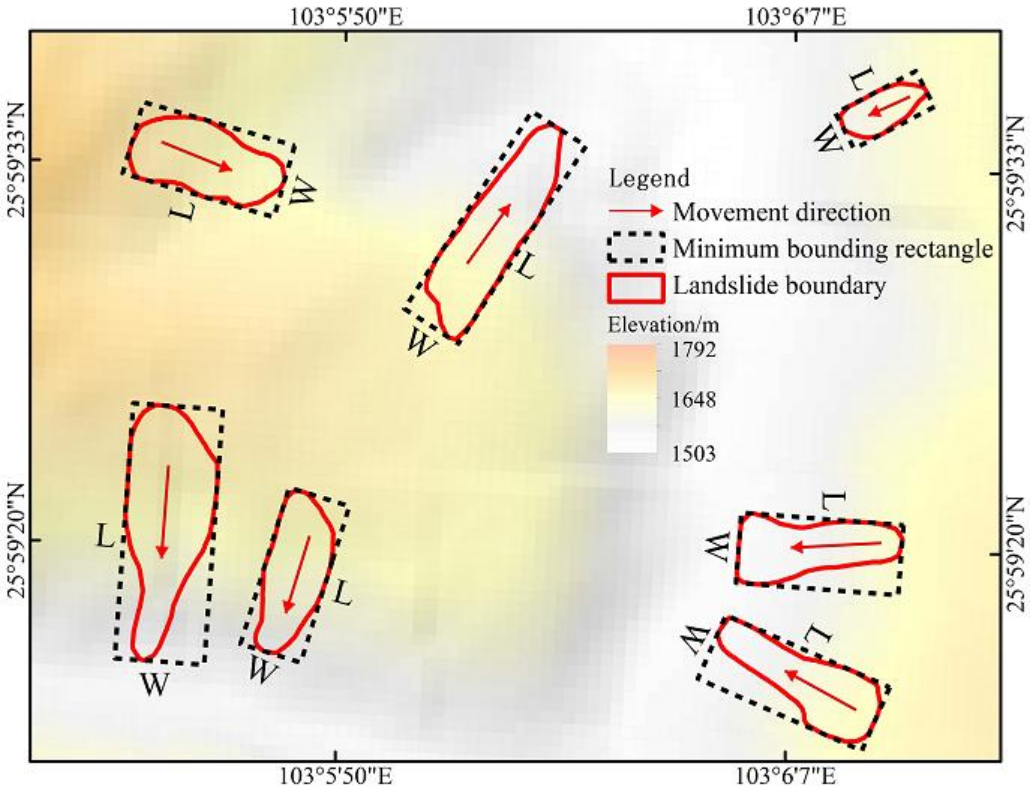

Figure 5. Sketch showing seven examples of landslide minimum bounding rectangles and siding directions that can be used to estimate the length and width of a landslide. These landslide boundaries were derived from the landslide inventory of the Dongchuan District.

3.3. Data Source

Various factors influenced the spatial distribution of landslides, and the interactions between landslides and these influencing factors can vary significantly across different regions [3–5]. This study investigated the impact of eight factors (elevation, slope, aspect, topographic relief, rainfall, distance to river and faults, and lithology) on the spatial distribution of landslides. A 12.5 m resolution ALOS PALSAR DEM served as the foundational data source. From this DEM, we extracted elevation (Figure 6a), slope (Figure 6b), aspect, topographic relief (Figure 6c), and river networks. Annual average rainfall (Figure 6d) data was derived by interpolating annual average precipitation data from stations surrounding the study area. Lithology and fault data were obtained from the 1:200,000-scale Geological map (http://dcc.cgs.gov.cn/). Distance to river and faults (Figure 6e-f) was calculated using ArcGIS's spatial analyst tool, measuring the distance from each grid cell center to the nearest river and fault. All of the influencing factor layers were transformed into raster format with a grid size of 12.5 × 12.5 m. These layers are illustrated in Figure 6. This paper calculates the the landslide number density (LND), and landslide area density (LAD) for each influencing factor. Detailed descriptions and calculation methods can be found in previous studies [38–41].

 doi:10.20944/preprints202603.0694.v1

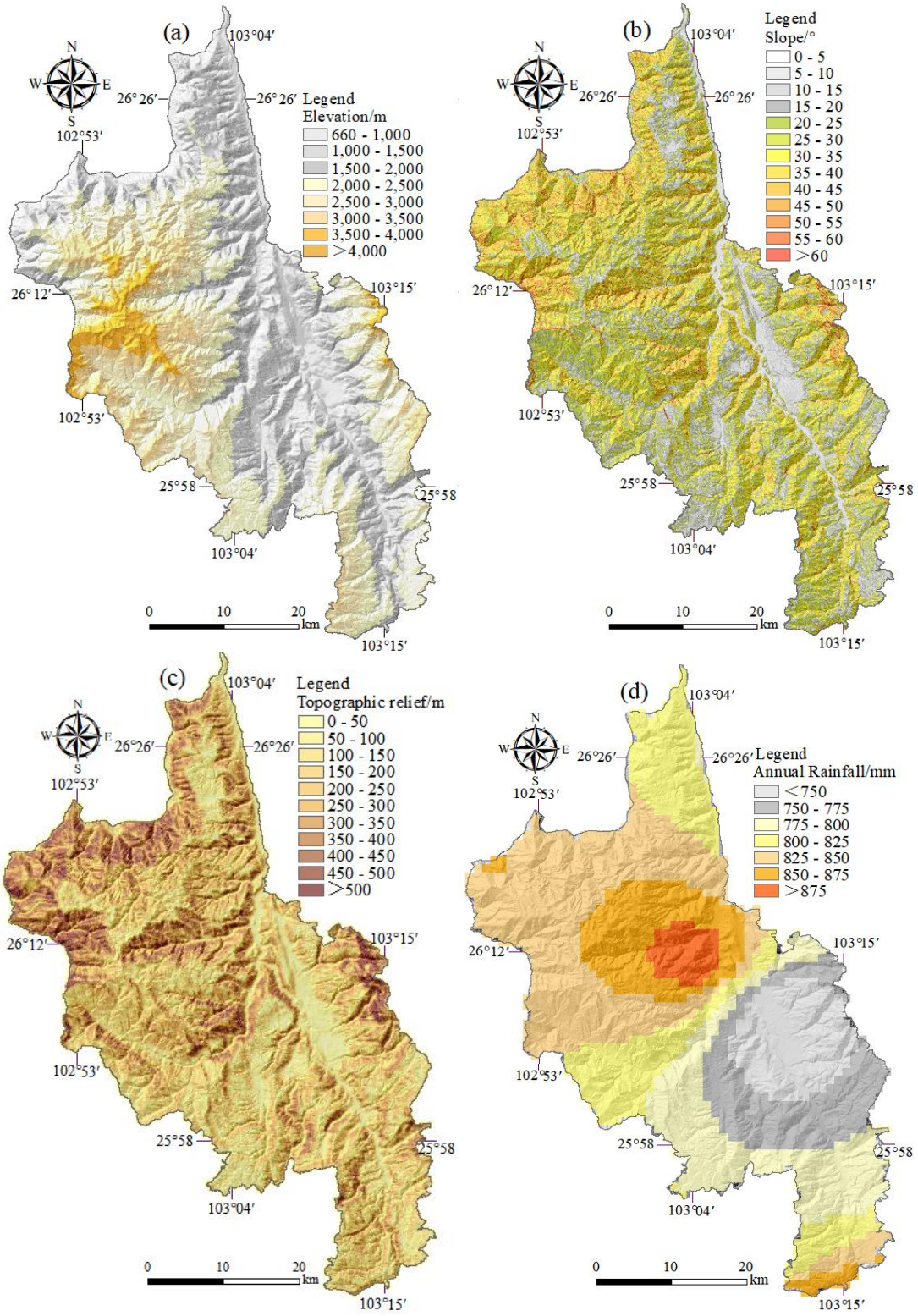

 doi:10.20944/preprints202603.0694.v1

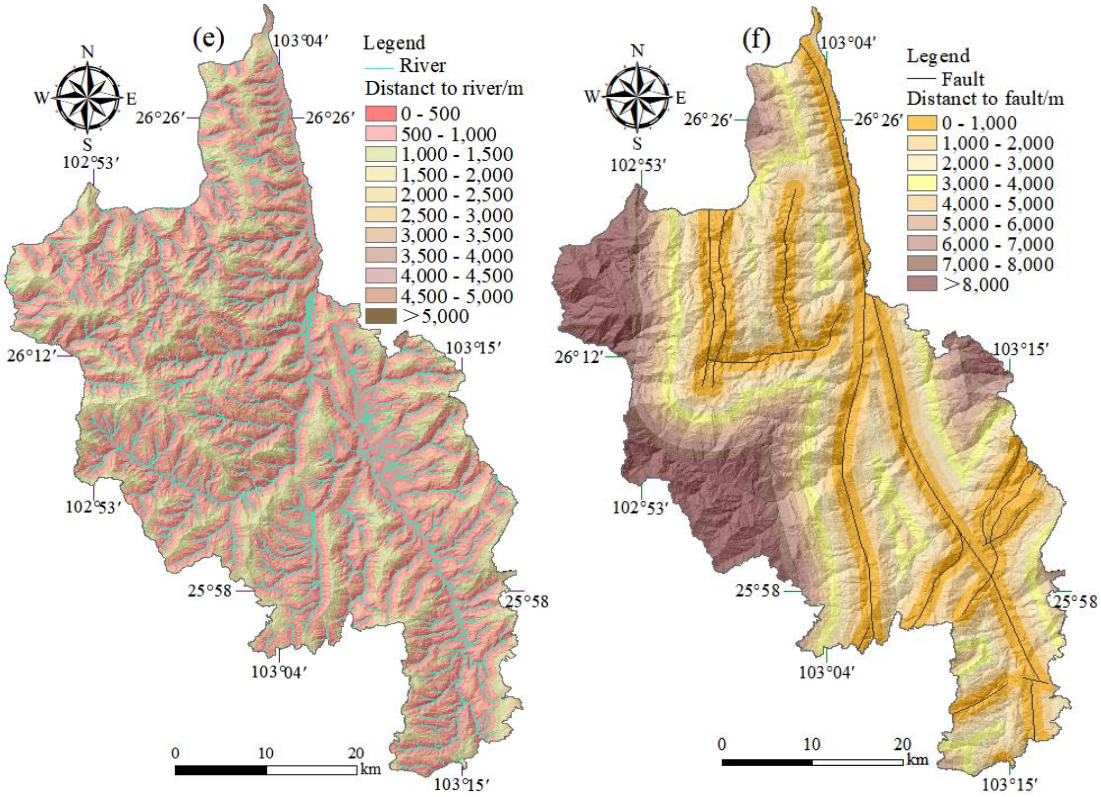

Figure 6. Maps showing the spatial distribution of influencing factors in the study area. (a) Elevation; (b) Slope angle; (c) Topographic relief; (d) Annual rainfall; (e) Distance to rivers; (f) Distance to faults. Green lines represent rivers and black lines denote faults.

4. Result

4.1. Landslide Inventory Map

Detailed and accurate landslide inventory maps are crucial for analyzing landslide spatial patterns [42,43]. In this study, a total of 1,623 landslides were identified, covering a cumulative area of 10.36 km²(Figure 7). Individual landslide areas ranged from 74.8 m²to 279,181 m², with an average of 6,384 m². Based on the empirical volume formula [30] and size classification criteria [44], 346 landslides (21.32%) had volumes between10^1 to 10^3 m^3, while 1,273 landslides (78.43%) ranged from 10^3 to 10^6 m^3, and only 4 landslides (0.25%) had volumes between 10^6 to 10^9 m^3. Consequently, medium-sized landslides predominated, followed by small-sized ones. According to the updated Varnes classification [45], the predominant types were debris flows and shallow surface landslides, followed by fewer instances of rock topples and rockslides.

 doi:10.20944/preprints202603.0694.v1

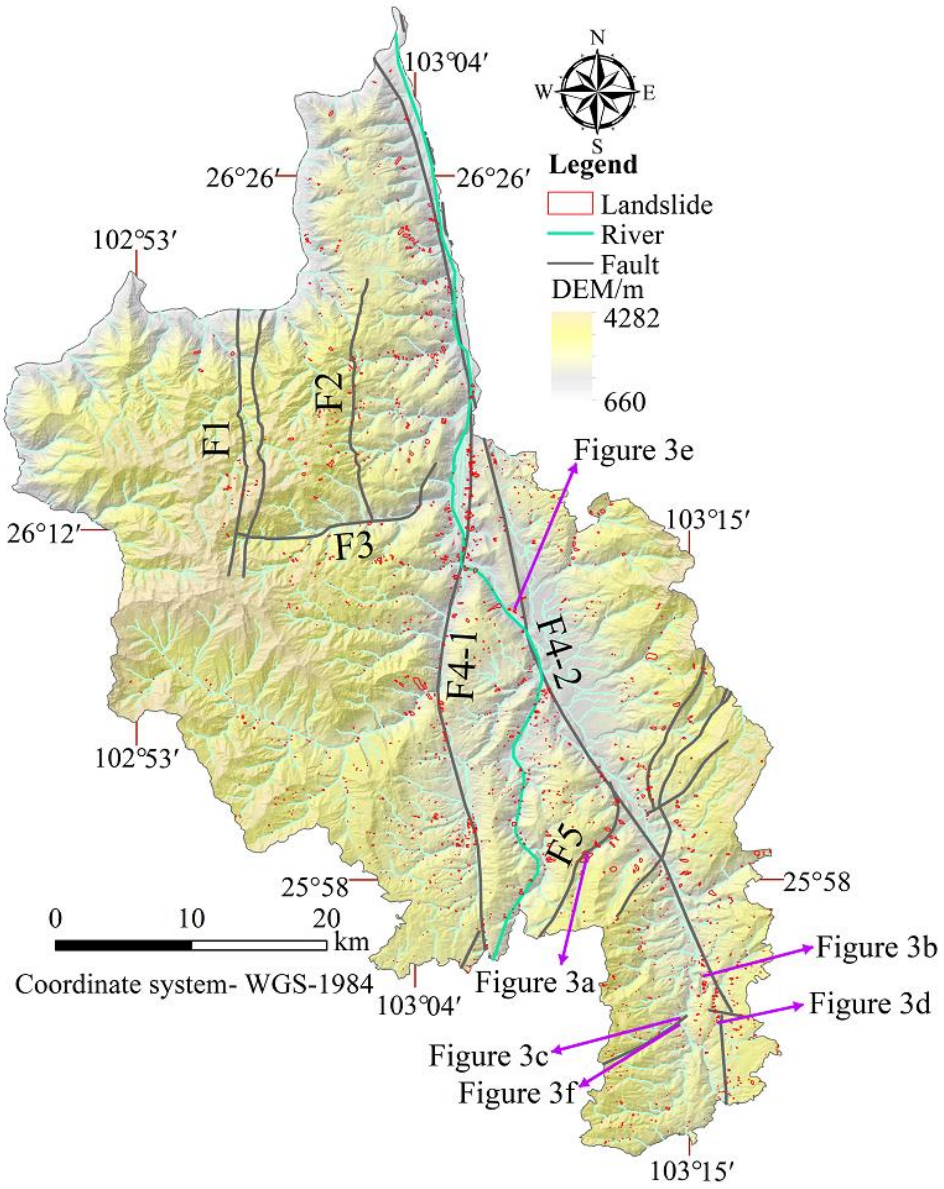

Figure 7. Landslide inventory map of the Dongchuan District. Red polygons denote landslides and black lines denote faults. Figures 3a-e show typical landslide positions.

Figure 8 illustrates the probability density distribution of landslide areas in log-log coordinates. The distribution curve follows an inverse gamma pattern, exhibiting a pronounced inflection point at an area of approximately 10^2 to 10^3 m^2. Beyond this point, the probability density decreases gradually with increasing landslide area. This observed pattern suggests that the identification and interpretation of the landslides were thorough and comprehensive [46].

 doi:10.20944/preprints202603.0694.v1

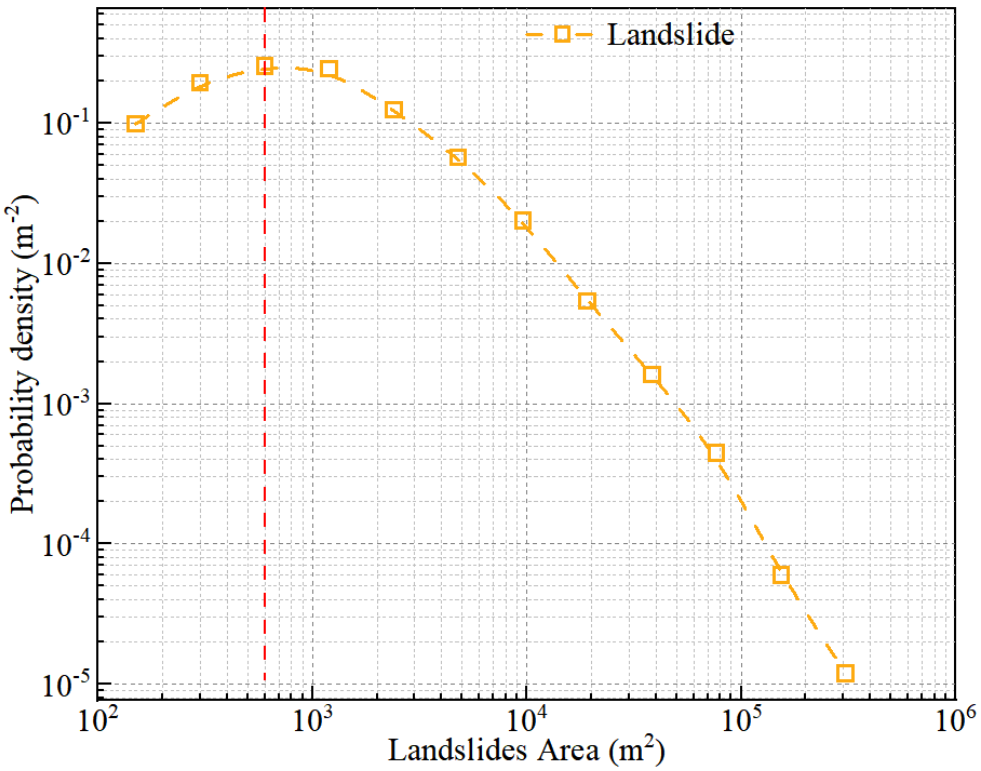

Figure 8. Probability density plot of landslide size (area in m²) distribution for the whole landslide inventory, The red line indicates the inflection point.

4.2. Spatial Distribution Characteristic of Landslides

Figure 9 reveals that landslides in the Dongchuan District exhibit a clustered distribution pattern, primarily concentrated in the central and southeastern parts of the study area. Regions adjacent to the Xiao River Fault (F4-1 and F4-2) are identified as areas with particularly high landslide density (Figure 10). In terms of scale, larger landslides with areas exceeding 0.01 km² are predominantly distributed along both sides of these fault segments.

The landslide number density (LND) and landslide area density (LAD) for the study area were calculated using the kernel density analysis tool in ArcGIS, with a moving window radius of 2.5 km (Figure 10a-b). The resulting maps show distinct distribution patterns, with peak values of 5.52 landslides/km² and 6.99%, respectively. Interestingly, the spatial distributions of LND and LAD show similarities, with their highest values generally co-located near major faults. Specifically, the highest LND (5.52 landslides/km²) is observed along the western (F4-1) and eastern (F4-2) branches of the Xiao River Fault, while the corresponding LAD in this area is only 2.36% (Figure 10a). This disparity suggests a concentration of smaller landslides. Conversely, the highest LAD (6.99%) occurs in the central part of the study area, near the western branch of the Xiao River Fault (F4-1) and the Yulu-Daibu Fault (F5) (Figure 10b). This area has a moderate associated LND of only 2.41 landslides/km², indicating a propensity for larger landslides.

 doi:10.20944/preprints202603.0694.v1

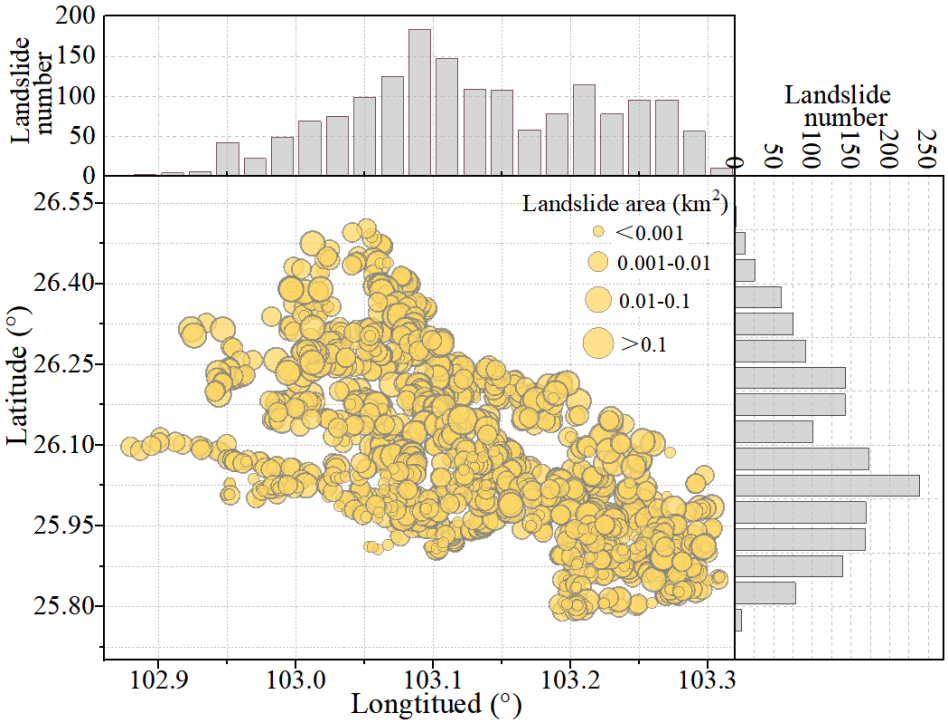

Figure 9. Spatial distribution and scales of landslides in the Dongchuan District along with their corresponding longitudinal and latitudinal profiles.

 doi:10.20944/preprints202603.0694.v1

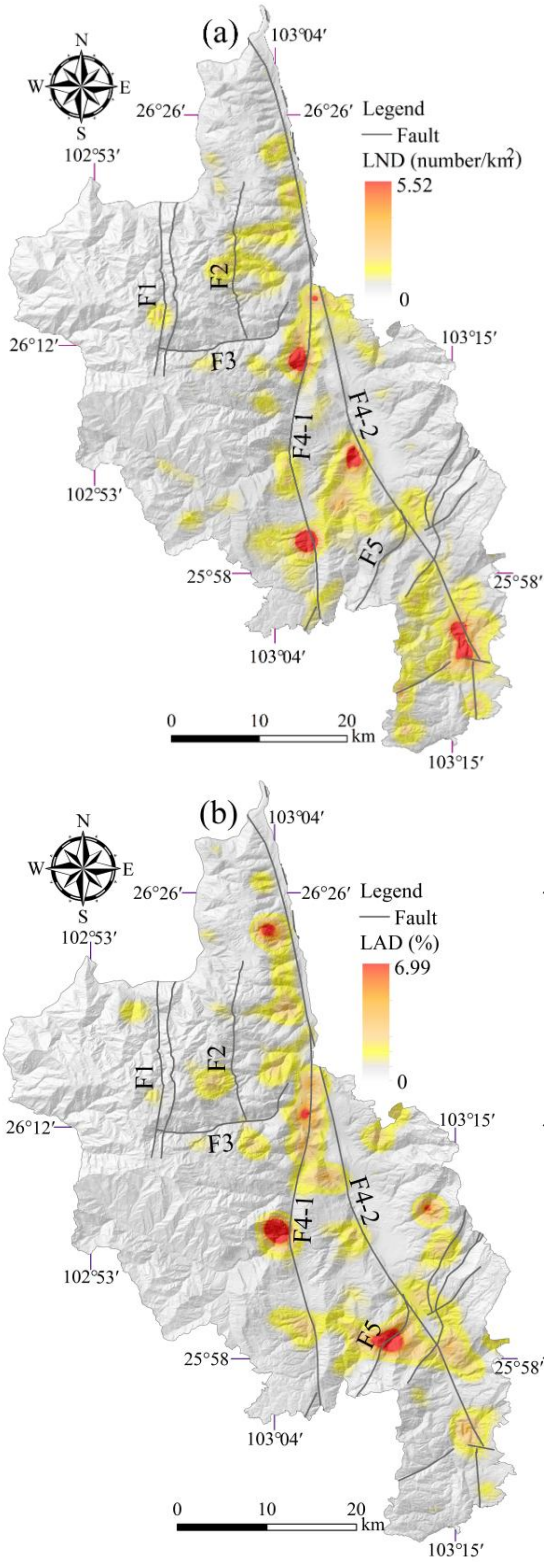

Figure 10. Map showing the spatial density distribution of landslides in the Dongchuan District. (a) Landslide number density (LND), (b) Landslide areal density (LAD). Densities are displayed by different background colors, with red indicating higher density and gray indicating lower density.

4.3. Relationship Between Landslide and Various Influencing Factors

Figure 11 illustrates the relationship between landslide abundance (LND and LAD) and various influencing factors. Regarding elevation, both LND and LAD showed an initial increase followed by a decrease with rising elevation. Landslide areas were predominantly concentrated within the 1,000-2,000 m range, accounting for 74.45% of the total area. The maximum LND and LAD of 1.41

 doi:10.20944/preprints202603.0694.v1

number/km², 1.11% occurred between 1,000 and 1,500 m (Figure 11a). For slope, the distribution of landslide areas followed a pattern similar to that of elevation. Most landslide areas were found on slopes between 20° to 45°, comprising 75.23% of the total. LND peaked at 1.20 number/km²within the 30°-35° range, while LAD reached its maximum of 1.14% between 55°-60° (Figure 11b). In terms of topographic relief, landslide areas were mainly distributed within the 150-400 m range, representing 64.1% of the total. Both LND and LAD tended to rise with increasing relief, reaching maxima of 1.22 number/km² at 200-250 m and 0.83 % at 450-500 m (Figure 11c). Regarding rainfall, landslides were predominantly found in areas with annual rainfall between 750 and 825 mm, accounting for 57.90% of the total landslide area. The highest LND and LAD of 1.31 number/km², 0.97% were observed in the 775-800 mm and 750-775 mm ranges, respectively (Figure 11d). For distance to rivers, most landslide areas were located within a distance of 1,000 m from river, comprising 90.87% of the total landslide area. Both LND and LAD decreased clearly as distance increased. The maximum LND of 4.0 number/km² occurred at 3,000-3,500 m from rivers, while the highest LAD of 0.81% was found within 0-1,000 m (Figure 11e). The trend for distance to faults was similar to that for rivers. Landslides were mainly distributed within 3,000 m of faults, making up 80.08% of the total. The highest values of LND and LAD, 1.32 number/km² and 0.88% were recorded at the distance of 0-1,000 m from the faults (Figure 11f).

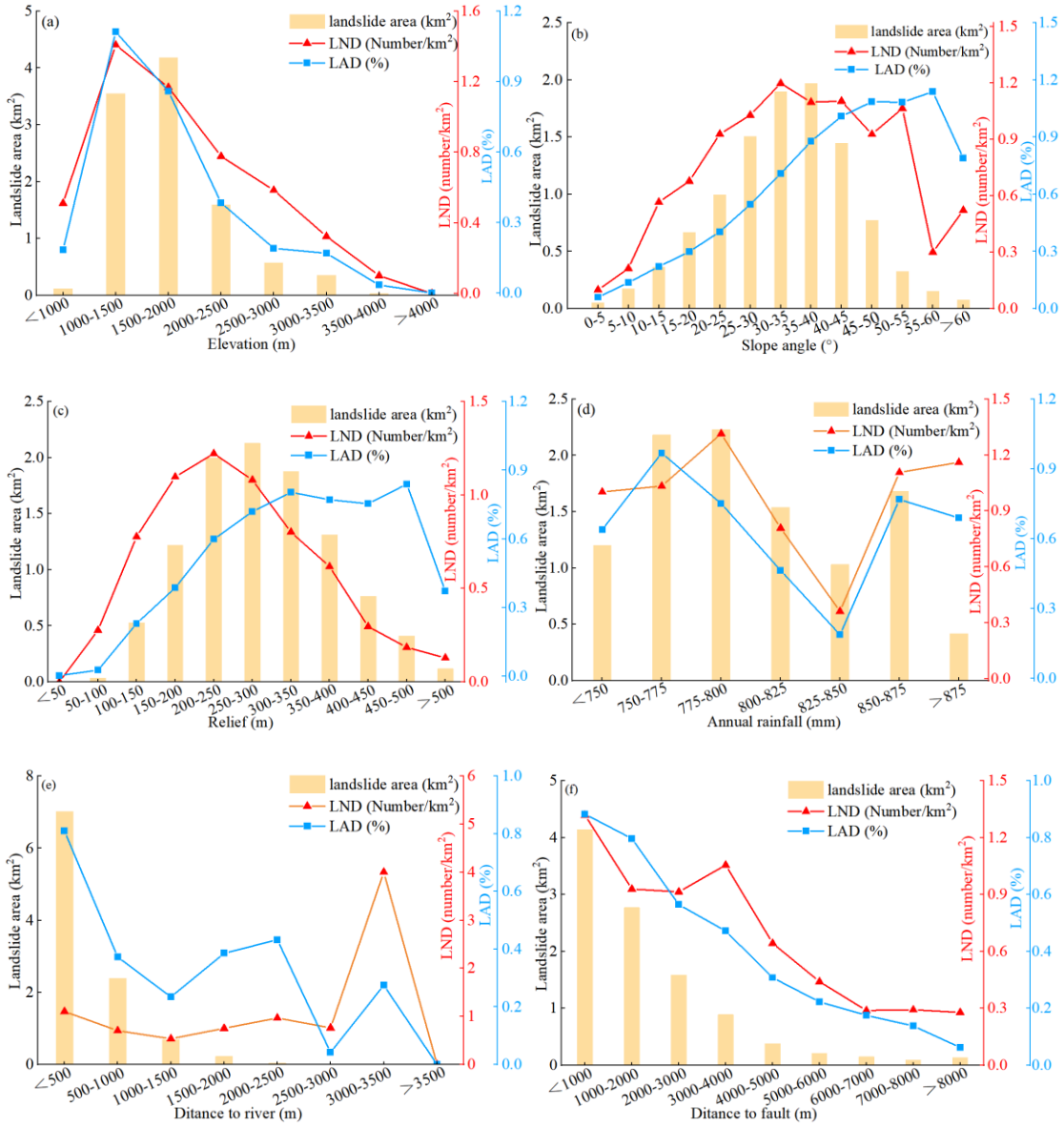

Figure 11. Correlations between landslide abundance indices (LND and LAD) and different influencing factors. (a) Elevation; (b) Slope; (c) Topographic relief; (d) Annual rainfall; (e) Distance to rivers; (f) Distance to faults.

 doi:10.20944/preprints202603.0694.v1

Figure 12 illustrates the distribution of landslides and the landscape (non-landslide) area ratio across different slope aspects. The landscape areas show a relatively uniform distribution, with area ratio in each aspect remaining around 0.04%. In contrast, landslide areas are predominantly concentrated on slopes facing 225°-315°. Notably, within the 255°-285° range, the landslide area ratio peaks at 0.068%. This indicates a strong tendency for landslides to occur on southwest-facing slopes.

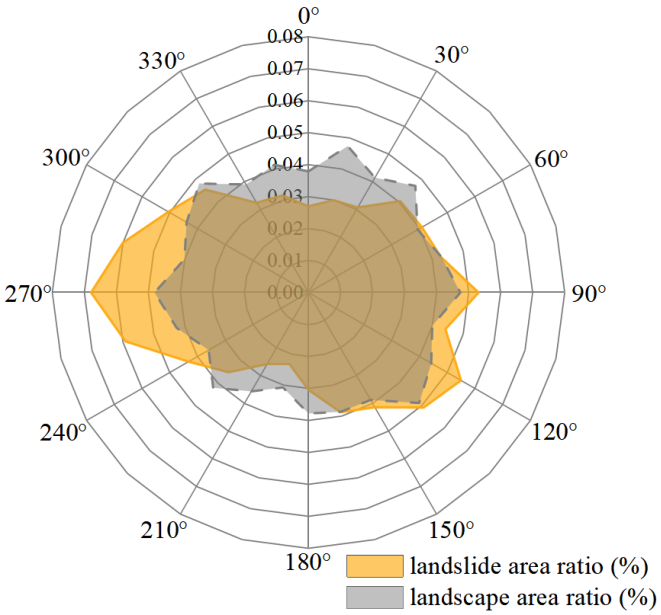

Figure 12. Distribution of slope aspects for landslides and landscape area. Yellow represents landslide areas and gray represents landscape areas.

Stratigraphic lithology serves as the foundational medium for landslide initiation. Figure 13 shows the area coverage proportions (%) of landslides, landscape regions, and the corresponding LAD across different lithological units. Among these, the Proterozoic (Pt) unit is the most extensive, covering 48.01% of the total study area and encompassing 50.09% of all landslides. The Permian (P) and Cambrian (Є) units rank second and third in landslide area, accounting for 30.30% and 9.38% of the total landslide area, respectively. In terms of LAD, the Paleozoic (Pz), Carboniferous (C), and Cambrian (Є) units exhibit relatively high values compared to other units. Notably, the Paleozoic (Pz) unit shows the highest LAD at 1.49%, indicating a higher susceptibility to landslides associated with this lithology.

 doi:10.20944/preprints202603.0694.v1

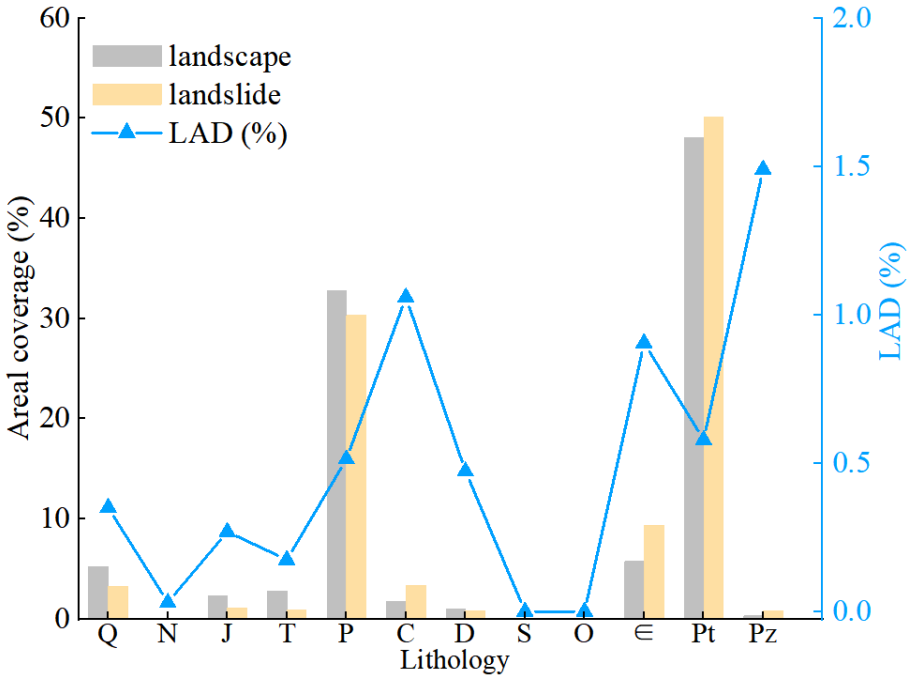

Figure 13. Distribution of areal coverage (%) for landslide and non-landslide areas, and landslide areal density (LAD) in different lithological units.

4.4. Geometric Characteristics of Landslides

The geometric parameters of landslides are commonly used to characterize their type and kinematic attributes. Figure 14 shows the frequency distribution of length-to-width (L/W) ratios for landslides in the study area. Overall, the L/W ratios range from 1.0 to 7.2, with a mean of 2.06. Approximately 76.96% of the landslide exhibit ratios between 1.2 and 3.0, 12.14% have ratios greater than 3.0, and 10.90% fall between 0.8 and 1.2. Based on the classification criteria for landslide geometrical characteristics [28], the majority of landslides can be categorized as longitudinal landslides ($1.2 \leq L/W < 3.0$), followed by elongated landslides ($L/W > 3.0$) and isometric landslides ($0.8 \leq L/W < 1.2$).

 doi:10.20944/preprints202603.0694.v1

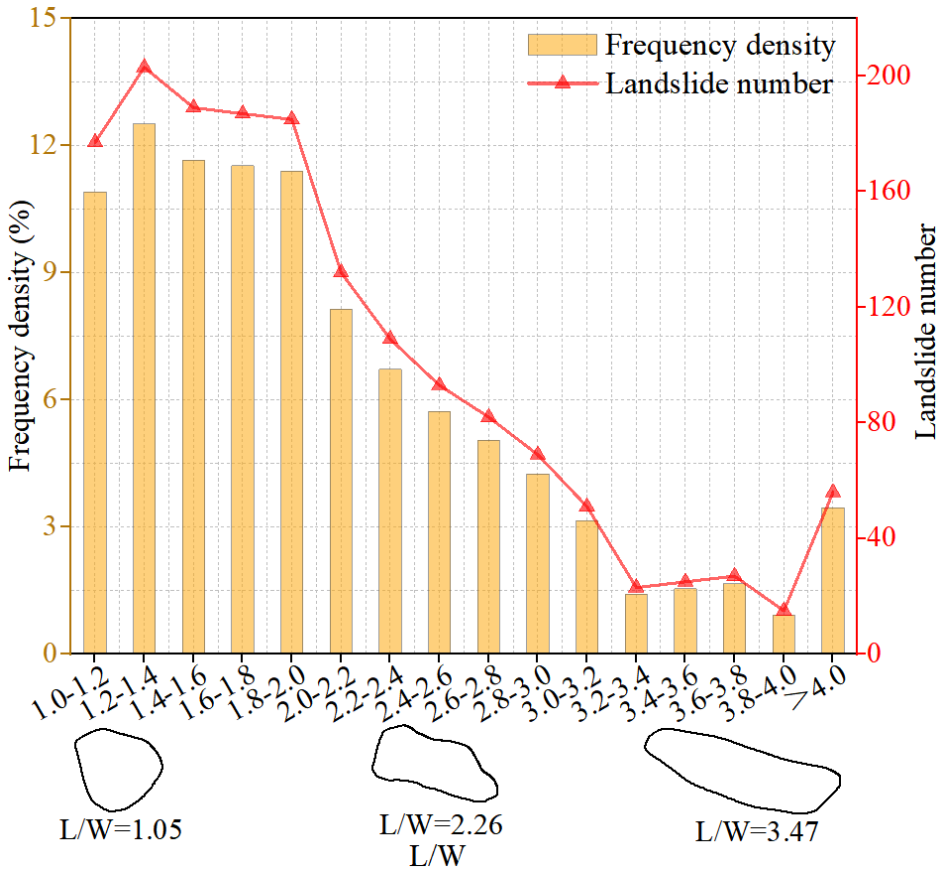

Figure 13. Map showing elongation ratio (L/W) of landslide planimetric shapes.

The geometric parameters of landslides are widely used to characterize their planar morphology and kinematic features, playing a key role in understanding landslide movement mechanisms [27,28]. Figure 14 illustrates the relationships among landslide travel distance (L), height (H), and volume. The travel distances (L) range from 11 to 1,068 m, with a mean value of 102 m, and are mainly clustered between 50 and 450 m. landslide heights (H) range from 1 to 782 m, with an average of 62 m, and are primarily concentrated between 25 and 350 m. Both L and H exhibit allometric scaling with volume (Figures 14a-b), expressed as: $L=3.16\times Volume^{0.38}$ ($R^2=0.90$) and $H=1.30\times Volume^{0.43}$ ($R^2=0.82$). Furthermore, travel distances (L) also increase allometrically with height (H) (Figure 14c), following $L=3.16\times H^{0.85}$ ($R^2=0.87$). These findings indicate that both landslide travel distance (L) and height (H) increase allometrically with volume, and that travel distance also increases allometrically with height.

 doi:10.20944/preprints202603.0694.v1

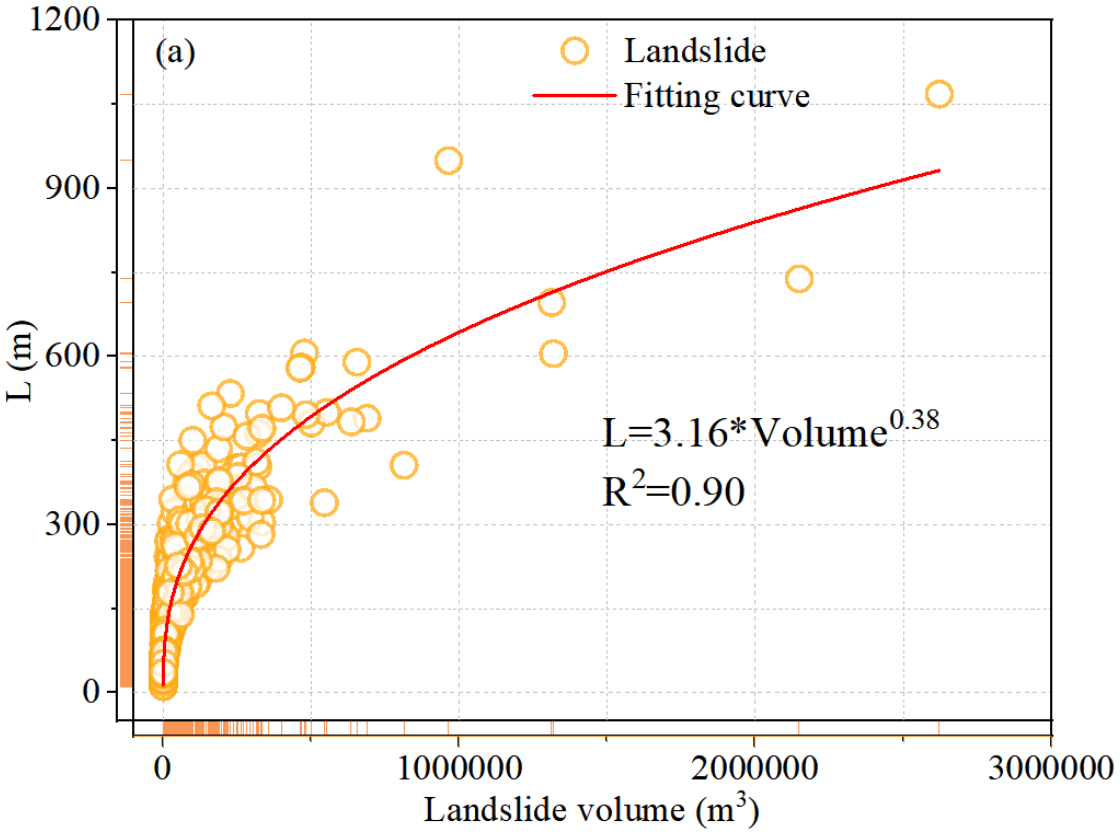

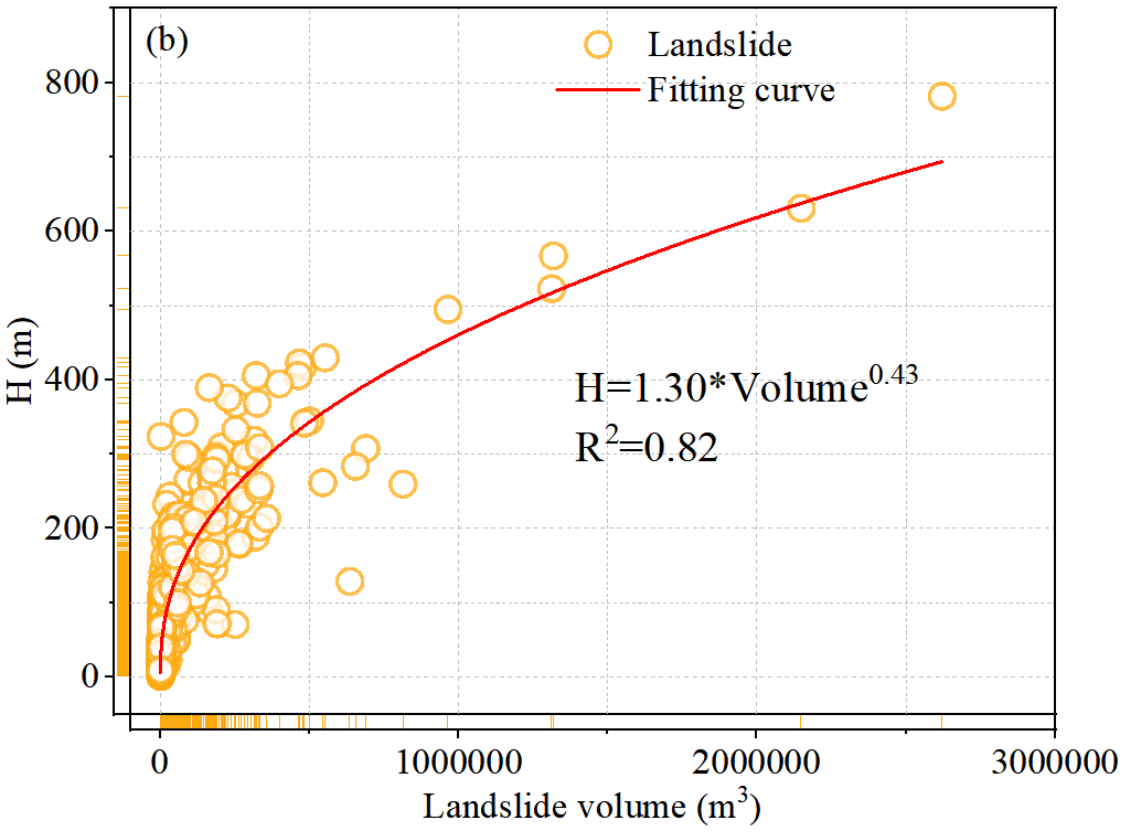

 doi:10.20944/preprints202603.0694.v1

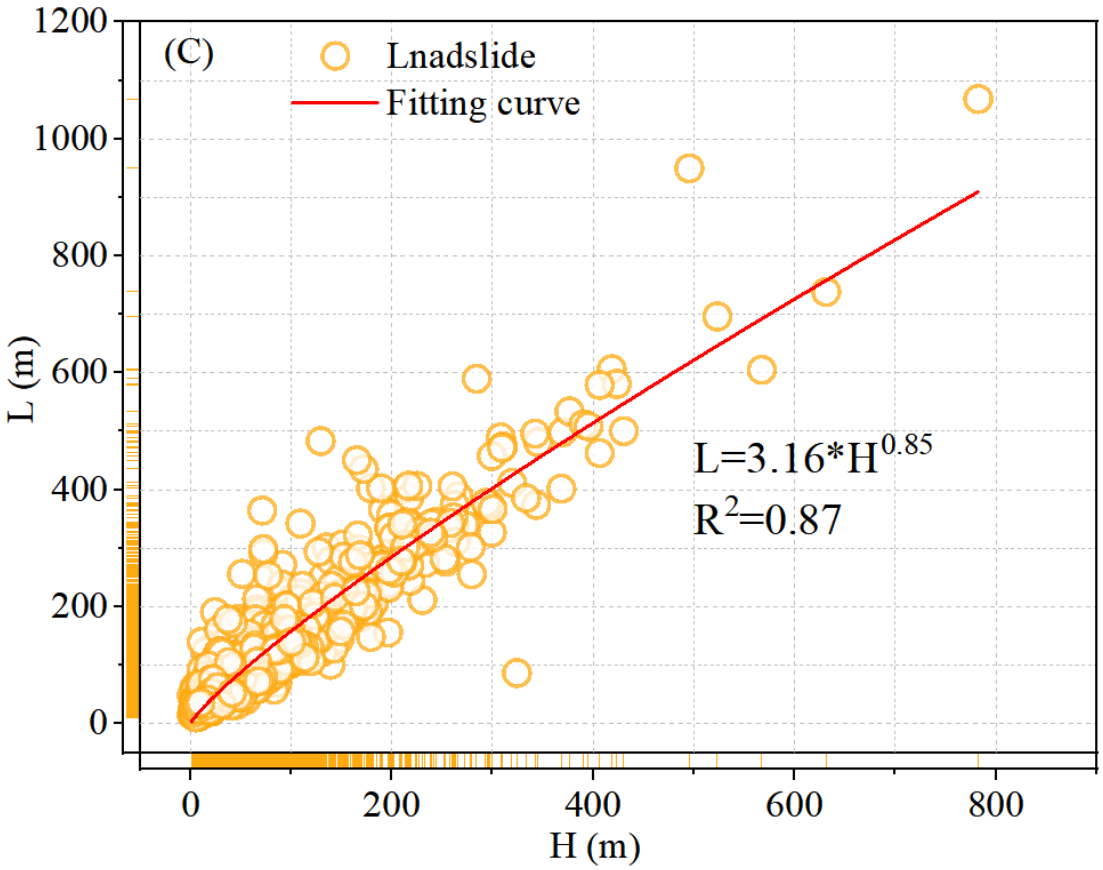

Figure 14. Mobility characteristics of landslides. (a) Relationship between Length (L) and landslide volume; (b) Relationship between height (H) and landslide volume; (c) Relationship between Length (L) and height (H).

5. Discussion

5.1. Controlling Factors Affecting the Distribution of Landslides

Understanding the spatial characteristics of landslides requires a comprehensive analysis of their complex interactions with topography. In this study, landslides in the Dongchuan District exhibit a distinct distribution pattern, with approximately 62.7% of them concentrated at elevations between 1,000 and 2,000 meters (Figure 15). Slope angle is a key indicator of a slope's potential energy and directly influences the scale of potential landslide events [47]. The majority of landslide were distributed within slope angles of 20° to 40°, accounting for 66.5% of the total landslide number (Figure 15). While landslides frequency show a relatively uniform distribution across aspects ranging from 0° to 300°, landslide are predominantly concentrated in the aspects of 60°-120° and 240°-300° (Figure 15). This pattern is attributed to higher rainfall intensities in these directions, influenced primarily by moisture transport from the Indian Ocean to the south. The combined effects of rainfall loading and hydro-mechanical softening drive slope instability in these aspects. Topographic relief is another important factor influencing landslide distribution, with 66.2% of all landslides occurring in areas with relief between 150 and 300 m, indicating higher susceptibility in these regions (Figure 15). Rainfall is a primary trigger of landslides [48]. The Dongchuan District receives abundant rainfall, and 54.9% of landslides are located in areas with annual precipitation between 750 and 825 mm (Figure 15). Rainfall undermines slope stability by facilitating water infiltration through surface cracks, which reduces the shear strength of soils and thereby increases slope susceptibility. In terms of distance to rivers, 86.8% of landslides occur within a distance of 1,000 m from river (Figure 15). Similarly, 73.9% of landslides are distributed at the distance of 3,000 m from the fault lines (Figure 15).

 doi:10.20944/preprints202603.0694.v1

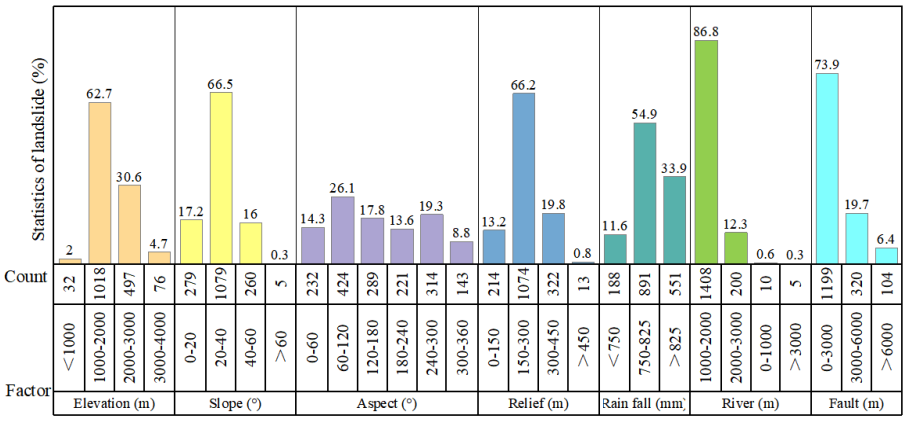

Figure 15. Statistical analysis of landslide influencing factors in the Dongchuan District.

5.2. Spatial Distribution Characteristic of Landslides

Faults play a crucial role in landslide occurrence, not only by weakening the integrity of slope rock masses but also by triggering seismic events [22]. This is evidenced by the clustering of landslides along the Xiao River Faults (F4-1, F4-2) (Figure 16a). Based on the landslide number density (LND), four distinct landslide clustering zones were identified (Figure 16b-e) using the natural breaks classification method. A density threshold of 2 number/km^2 was used to delineate the boundaries of these clusters, while 4 number/km^2 was used to distinguish between medium- and high-density clusters. Zone A positioned in the middle segment of the Western Branch of the Xiao River Fault (F4-1), where an earthquake of *M*s 6.5 has occurred, and it exhibits the highest LND and LAD values of 4.89 number/km^2 and 4.28%, respectively (Figure 16b), with a total of 115 landslides. Elevations in this zone range from 1,038 to 2,017 m, with an average slope of 22.87°, and a topographic relief of 6-494 m. Zone B lies in the southern part of the Western Branch of the Xiao River Fault (F4-1) and contains 53 landslides, with maximum LND and LAD values of 5.52 number/km^2 and 2.36%, respectively (Figure 16c). Elevations range from 1,419 to 2,051 m, with a mean slope of 23.70° and relief ranging from 31 to 442 m. Zone C is found near the middle segment of the Eastern Branch of the Xiao River Fault (F4-2) and shows LND and LAD values of 4.50 number/km^2 and 1.86% (Figure 16d), also containing 118 landslides. The elevation ranges from 1,097 to 2,138 m, with an average slope of 21.82° and relief between 8 and 457 m. Zone D is located in the southern part of the Eastern Branch of the Xiao River Fault (F4-2) and exhibits LND and LAD values of 4.45 number/km^2 and 3.06% (Figure 16e), with a total of 138 landslides. Elevations in this zone range from 1,401 to 2,468 m, with a mean slope of 23.21° and relief between 20 and 467 m. These four landslide clustering zones along the Xiao River Fault (F4-1, F4-2) highlight the significant influence of the fault on the spatial distribution of landslides. As an active fault, the Xiao River Fault creates unfavorable geological conditions, reducing rock mass strength and promoting crack development, Consequently, water infiltrates the rock mass through existing fractures. As pore water pressure increases and the shear strength of potential sliding surfaces decreases [48], the area becomes highly susceptible to landslides.

 doi:10.20944/preprints202603.0694.v1

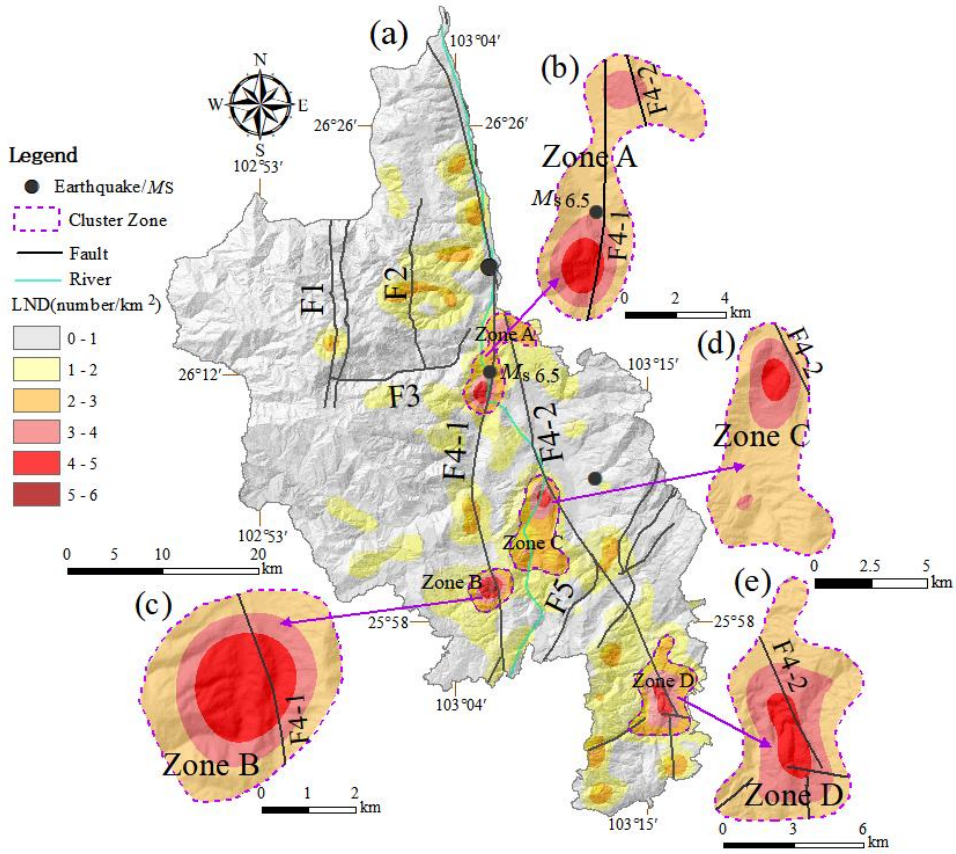

Figure 16. Map showing spatial clustering analysis of landslides in the Dongchuan District. Based on landslide number density (LND), four clustering zones were identified (Figure 16b-e). LND is displayed by background colors, with red indicating high density and gray indicating low density.

5.3. Comparative Analysis with Other Regions

The northeastern and western regions of Yunnan Province are recognized as typical areas of prominent landslide hazard due to their distinctive alpine canyon terrain, making them a focus of scientific research. However, systematic comparative studies on the spatial distribution patterns and geometric characteristics of landslides in these two regions remain scarce. This paper bridges this gap through a comprehensive comparative analysis. Landslides in the Dongchuan District predominantly occur at higher elevations (1,000-2,000) and on steeper slopes (20°-45°). In contrast, recent landslides in Baoshan City, located in western Yunnan Province, are concentrated at lower elevations (1,680-1,798 m) and on gentler slopes (15°-40°) [7]. The average H/L ratio in the study area is 0.56 (corresponding to a mean reach angle of 29°), which is higher than that in Baoshan City, where the average H/L ratio is 0.4 (mean reach angle 21°) [7]. These differences can be attributed to the fact that, although both areas share high-relief canyon terrain, the Dongchuan District situated along the Xiao River Fault Zone, one of the most seismically active faults in southwestern China, where frequent and intense seismic activities occur. Earthquakes damage and weaken structural discontinuities in rock and soil masses on slopes, as well as promote fracture development, creating unfavorable geological conditions for landslides. Furthermore, the Dongchuan District has a long history of copper mining [49], and anthropogenic activities have severely disturbed both surface and subsurface geological environments. Moreover, the district has low vegetation coverage, severe soil erosion, and a fragile ecosystem, resulting in loose structures of slope rock and soil with consequently reduced shear strength. Under heavy rainfall, unstable rock and soil masses on slopes are susceptible to long-distance transport along gullies. The combined effects of these factors result in a landslide type in the study area dominated by debris flows, with shallow surface landslides as the secondary

 doi:10.20944/preprints202603.0694.v1

type; landslide morphology is mainly longitudinal, and the average H/L ratio is significantly higher than that of Baoshan City.

Landslide mobility represents the run-out distance of a landslide [33] and is positively correlated with landslide volume [50]. In this study, the relationship between travel distance (L) and volume is expressed by the empirical formula: $L=3.16\times Volume^{0.38}$ ($R^2=0.90$). This reflects that travel distance (L) increases with volume following an allometric growth trend (Figure 14a), confirming that landslide volume significantly influences mobility.

This study reveals clustering of landslides along fault lines, confirming that faults play a critical role in the spatial distribution of landslides. However, quantitative investigations of fault activity remain insufficient, constraining precise quantification of landslide spatiotemporal distribution patterns. Furthermore, the spatial distribution and geometric characteristics of landslides are the cumulative result of long-term geomorphic and tectonic evolution. Future work will systematically investigate fault activity in the study area, with the aim of elucidating the coupled controlling mechanisms of tectonic activity, topographic conditions, and climate variability, on landslide formation and evolution across multiple spatiotemporal scales. Such efforts will provide a fundamental basis for deeper understanding of landscape evolution and for improving risk assessment of geological hazard chains along the northern margin of the Yunnan-Guizhou Plateau.

6. Conclusions

This study establishes a detailed landslide inventory for the Dongchuan District based on visual interpretation of high-resolution Google Earth imagery. Statistical analyses were conducted on landslide numbers, areas, and morphological parameters, and the relationships between landslide occurrence and various influencing factors were systematically analyzed. The main conclusions are as follows:

1. The landslide inventory for the Dongchuan District identified 1,623 landslides, covering a combined area of 10.36 km^2, with a mean area of 6,384 m^2. The majority were medium-sized, followed by small landslides. Landslides predominantly occurred in areas characterized by high elevation (1,000-2,000 m), steeper slopes (20°-45°), preferred slope aspects are 255°-285°, high relief (150-400 m), rainfall of 750-825 mm, and within a distance of 1,000 m from rivers and 3,000 m from fault lines. The lithological unit of Paleozoic (Pz) exhibited the highest landslide area density (LAD) value of 1.49%, indicating higher susceptibility to landslides. Kernel density analysis revealed four landslide clusters (Zones A-D) distributed along the Xiao River Fault (F4-1, F4-2), highlighting the significant influence of the fault on the spatial distribution of landslides.

2. Morphological analysis revealed that the majority of landslides in this study area were longitudinal in planform, with travel distances (L) of 50-450 m and heights (H) of 25-350 m. The relationships between H, L, and volume followed allometric trends: $L=3.16\times Volume^{0.38}$ ($R^2=0.90$), $H=1.30\times Volume^{0.43}$ ($R^2=0.82$), and $L=3.16\times H^{0.85}$ ($R^2=0.87$). These expressions demonstrated that both H and L increased with volume, and that L increased with H. The mean reach angle of 29° was significantly higher than that of Baoshan City (21°). These findings indicated that the landslide spatial distribution, geometry, and kinematics were significantly influenced by tectonics, topography, and geomorphology.

Acknowledgments: We thank Google Earth satellite images for the free access satellite images used in this study. This study was supported by The Science and Technology Special Program of Yunnan Earthquake Bureau (2025ZX04), and the National Nonprofit Fundamental Research Grant of China, Institute of Geology, China Earthquake Administration (Grant no. IGCEA2202).

Author Contributions: X.C. proposed the research concept, organized the landslide interpretation, and provided basic data. S.L. designed the framework and wrote the manuscript. S.M, participated in the writing and data analysis. ; Declarations Conflict of interest: The authors declare no competing interests.

References

 doi:10.20944/preprints202603.0694.v1

1. Burbank, D. W.; Rates of erosion and their implications for exhumation. Mineralogical Magazine. 2002, 66, 25-52.
2. Roering, J. J., Perron, J. T., Kirchner, J. W. Functional relationships between denudation and hillslope form and relief. Earth and Planetary Science Letters. 2007, 264, 245-258.
3. Gorüm, T. Tectonic, topographic and rock-type influences on large landslides at the northern margin of the Anatolian Plateau. Landslides. 2018, 16, 333-346.
4. Jacobs, L.; Dewite, O.; Poesen, I.; Maes, J.; Mertens, K.; Sekajugo, J.; Kervyn, M. Landslide characteristics and spatial distribution in the Rwenzori Mountains, Uganda. Journal of African Earth Sciences. 2017, 134, 917-930.
5. Tanyas, H.; Rossi, M.; Alvioli, M.; van, Westen, C. J.; Marchesini, I.; A global slope unit-based method for the near real-time prediction of earthquake-induced landslides. Geomorphology. 2019, 327, 126-146.
6. Santangelo, M.; Gioia, D.; Cardinali, M.; Guzzetti, F.; Schiattarella, M.; Landslide inventory map of the upper Sinni River valley, Southern Italy. Journal of Maps. 2014, 11:444-453.
7. Shao, X.; Ma, S.; Xu, C.; Shen, L.; Lu, Y. Inventory, Distribution and Geometric characteristics of landslides in Baoshan City, Yunnan Province, China. Sustainability. 2020, 12, 24-33.
8. Cui, P.; He, M.; Tapponnier, P.; Zhang, L.; Li, Z.; Gong, W.; Zhou, G.; Guo, J.; Preface for Geohazards and mitigation along the Sichuan-Tibet Railway. Engineering Geology. 2023, 317, 107095.
9. Tian, Y.; Xu, C.; Xu, X.; Wu, S. E.; Chen, J. Spatial distribution analysis of coseismic and pre-earthquake landslides triggered by the 2014 Ludian MS 6.5 earthquake. Seismology and Geology. 2015, 37, 291-306.
10. He, X.; Xu, C.; Qi, W.; Huang, Y.; Cheng, J.; Xu, X.; Yao, Q.; Lu, Y.; Dai, B.; Landslides Triggered by the 2020 Qiaojia Mw 5.1 Earthquake, Yunnan, China: Distribution, Influence Factors and Tectonic Significance. Journal of Earth Science. 2021, 32, 1056-1068.
11. Jin, J. L.; Cui, Y. L.; Xu, C.; Zheng, J.; Miao, H. B. Application of logistic regression model for hazard assessment of landslides caused by the 2012 Yiliang Ms 5.7 earthquake in Yunnan Province, China. Journal of Mountain Science. 2023, 20, 657-669.
12. Tian, S.; Zhang, Z. Housing loss estimation study of urban debris flow disaster based on SPOT-5 data-A case study on Dongchuan District, Kunming, Yunnan Province. In 2009 Joint Urban Remote Sensing Event. IEEE. 2009, 1-5.
13. Cui, P.; Zou, Q.; Xiang, L.; Zeng, C. Risk assessment of simultaneous debris flows in mountain townships. Progress in physical geography. 2013, 37, 516-542.
14. Xu, J.; Cheng, X.; Huang, Q.; Chen, Y.; Qi, W.; Yuan, J.; Yang, J. Susceptibility evaluation of debris flow based on experience weight method combined with"3S"technology: a case study from Dongchuan in Yunnan Province, China. IOP Conference Series: Earth and Environmental Science. IOP Publishing. 2017, 95, 022051.
15. Li, K.; Zhao, J. S.; Lin, Y. L.; Chen, K., Bi, R. Assessment of debris flow susceptibility in Dongchuan based on RF and SVM models. Journal of Yunnan University: Natural Sciences Edition. 2021, 44, 107-115.
16. Sun, B.; Zhu C. B.; Kang, X. B.; Ye, L.; Liu，Y. Susceptibility assessment of debris flows based on information model in Dongchuan, Yunnan Province. The Chinese Journal of Geological Hazard and Control. 2022, 33, 119-127.
17. Wei, F.; Hu, K.; Cui, P.; Guan, Q. A decision support system for debris-flow hazard mitigation in towns based on numerical simulation: a case study at Dongchuan, Yunnan Province. International Journal of Risk Assessment and Management. 2008, 8, 373-383.
18. Cao, C.; Song, S.; Chen, J.; Zheng, L., Kong, Y. An approach to predict debris flow average velocity. Water. 2017, 9, 205.
19. Liu, D.; Li, Y.; You, Y.; Liu, J., Wang, B.; Yu, B. Velocity of debris flow determined by grain composition. Journal of Hydraulic Engineering. 2020, 146, 06020010.
20. Zhang, X.; Gan, S.; Yuan, X.; Zong, H.; Wu, X. Slope deformation monitoring and early identification of disasters in debris flow source area of Baini River, Dongchuan District, China. Frontiers in Earth Science. 2022, 10, 1000736.

 doi:10.20944/preprints202603.0694.v1

21. Shen, J.; Wang, Y. P.; Song, F. M. Characteristics of the active Xiaojiang fault zone in Yunnan, China: a slip boundary for the southeastward escaping Sichuan-Yunnan Block of the Tibetan Plateau. Journal of Asian Earth Sciences. 2003, 21, 1085-1096.
22. Li, C.; Zhang, J.; Gao, L.; Chen, X.; Ma, S.; Yuan, R. Spatial Clustering and distribution characteristics of large landslides in the Yalong River Basin, China. Geomorphology. 2025, 109667.
23. Bian, M.; Qiu, H.; Chen, X. The Distribution Characteristics of Large Landslides Along the Daduhe River in the Eastern Tibetan Plateau and Their Effects on Landscape Evolution. Remote Sensing. 2025, 17, 1133.
24. Ma, S. Y.; Shao, X. Y.; Xu, C. Landslide inventory and distribution patterns in Lhasa area, Tibet Plateau. Natural Hazards. 2025, 121, 5849-5871.
25. Guzzetti, F.; Mondini, AC.; Cardinali, M.; Fiorucci, F.; Santangelo, M.; Chang, K-T. Landslide inventory maps: New tools for an old problem. Earth-Science Reviews. 2012, 112, 42-66.
26. Xu, C. Preparation of earthquake-triggered landslide inventory maps using remote sensing and GlS technologies: Principles and case studies. Geoscience Frontiers. 2015, 6, 825-836.
27. Taylor, F, E.; Malamud, B, D.; Witt, A.; Guzzetti F. Landslide shape, ellipticity and length-to-width ratios. Earth Surface Processes and Landforms. 2018, 43, 3164-3189.
28. Tian, Y.; Xu, C.; Chen, J.; Zhou, Q.; Shen, L. Geometrical characteristics of earthquake-induced landslides and correlations with control factors: a case study of the 2013 Minxian, Gansu, China, Mw 5.9 event. Landslides. 2017, 14, 1915-1927.
29. lAEG. Commission on Landslides. Suggested nomenclature for landslides. Bulletin of the International Association of Engineering Geology-Bulletin de l'Association Internationale de Géologie de l'Ingénieur. 1990, 41, 13-16.
30. Larsen, I, J.; Montgomery, D, R.; Korup, O. Landslide erosion controlled by hillslope material. Nature Geoscience. 2010, 3, 247-251.
31. Xu, C.; Xu, X.; Shen, L.; Yao, Q.; Tan, X.; Kang, W.; Ma, S.; Wu, X.; Cai, J.; Gao, M. Optimized volume models of earthquake-triggered landslides. Scientific Reports. 2016, 6, 29797.
32. Fan, X.; Scaringi, G.; Xu, Q.; Zhan, W.; Dai, L.; Li, Y.; Pei, X.; Yang, Q.; Huang, R. Coseismic landslides triggered by the 8 th August 2017 Ms 7.0 Jiuzhaigou earthquake (Sichuan, China): Factors controlling their spatial distribution and implications for the seismogenic blind fault identification. Landslides. 2018, 15, 967-983.
33. Roback, K.; Clark, M. K.; West, A . J.; Zekkos, D.; Li, G.; Gallen, S. F.; Chamlagain, D.; Godt, J.W. The size, distribution, and mobility of landslides caused by the 2015 Mw7. 8 Gorkha earthquake, Nepal. Geomorphology. 2018, 301, 121-138.
34. Zou, Y.; Oi, S.; Guo, S.; Zheng, B.; Zhan, Z.; He, N.; Huang, X.; Hou, X.; Liu, H. Factors controlling the spatial distribution of coseismic landslides triggered by the Mw 6.1 Ludian earthguake in China. Engineering Geology. 2022, 296, 106477.
35. Huang, Y.; Xu, C.; He, X.; Cheng, J.; Huang, Y.; Wu, L.; Xu, X. Distribution characteristics and cumulative effects of landslides triggered by multiple moderate-magnitude earthquakes: a case study of the comprehensive seismic impact area in Yibin, Sichuan, China. Landslides. 2024, 21, 2927-2943.
36. Pourghasemi, H, R.; Moradi, H, R.; Aghda, S, M, F.; Sezer, E, A.; Jirandeh, A, G.; Pradhan, B. Assessment of fractal dimension and geometrical characteristics of the landslides identified in North of Tehran, Iran. Environmental Earth Sciences. 2013, 71, 3617-3626.
37. Hunter, G.; Fell, R.Travel distance angle for rapid landslides in constructed and natural soil slopes. Canadian Geotechnical Joural. 2003, 40, 1123-1141.
38. Xu, C. A preliminary spatial distribution analysis of landslides triggered by the 2010 Haiti earthquake. In Landslide Science for a Safer Geoenvironment: Volume 3: Targeted Landslides. Cham: Springer International Publishing. 2014, 183-190.
39. Tian, Y.; Xu, C.; Xu, X.; Chen, j. Detailed inventory mapping and spatial analyses to landslides induced by the 2013 Ms 6.6 Minxian earthquake of China. Journal of Earth Science. 2016, 27, 1016-1026.

 doi:10.20944/preprints202603.0694.v1

40. Tanyas, H.; Westen, c.; Allstadt, K.; jibson, R. Factors controlling landslide frequency-area distributions. Earth Surface Processes and Landforms. 2018, 44, 900-917.
41. Wang, W.; Ma, S.; Yan, W.; Yuan, R. The Spatial Distribution Characteristics and Possible Influencing Factors of Landslide Disasters in the Zhaotong Area, Yunnan Province of China. Applied Sciences. 2024, 14, 5093.
42. Bucci, F.; Santangelo, M.; Cardinali, M.; Fiorucci, F.; Guzzetti, F. Landslide distribution and size in response to Quaternary fault activity: the Peloritani Range, NE Sicily, Italy. Earth Surface Processes and Landforms. 2016, 41, 711-720.
43. Marc, O.; Hovius, N. Amalgamation in landslide maps: Effects and automatic detection. Natural Hazards and Earth System Science. 2015, 15, 723-733.
44. McColl, S.T.; Cook, S.J. A universal size classification system for landslides. Landslides. 2024, 21, 111-120.
45. Hungr, O.; Leroueil, S.; Picarelli, L. The Varnes classification of landslide types, an update. Landslides. 2014, 11, 167-194.
46. Malamud, B, D.; Turcotte, D, L.; Guzzetti F.; Reichenbach P. Landslide inventories and their statistical properties. Earth Surface Processes and Landforms. 2004, 29, 687-711.
47. Katz, O.; Morgan, J.K.; Aharonov, E.; Dugan, B. Controls on the size and geometry of landslides: Insights from discrete element numerical simulations. Geomorphology. 2014, 220, 104-113.
48. Barth, S.; Geertsema, M.; Bevington, A.R.; Bird, A.L.; Clague, J.J.; Millard, T.; Bobrowsky, P.T.; Hasler, A.; Liu, H. Landslide response to the 27 October 2012 earthquake (Mw 7.8), southern Haida Gwaii, British Columbia, Canada. Landslides. 2020, 17, 517-526.
49. Wang, T.; Liu, J.; Huang, C. Research on Ore-controlling factors and Metallogenic Prognosis of Dongchuan Copper Mining Area, Yunnan, China. In IOP Conference Series: Earth and Environmental Science. IOP Publishing. 2017, 59, 01203.
50. Scheidegger, A, E. On the prediction of the reach and velocity of catastrophic landslides. Rock Mechanics and Rock Engineering. 1973, 5, 231-236.